Barocaloric and Magnetocaloric Effects in $(MnNiSi)_{1-x}(FeCoGe)_x$

Tapas Samanta[1],[*] Pol Lloveras[2], Ahmad Us Saleheen[1], Daniel L. Lepkowski[1], Emily Kramer[1], Igor Dubenko[3], Philip W. Adams[1], David P. Young[1], Maria Barrio[2], Josep Ll. Tamarit[2], Naushad Ali[3], and Shane Stadler[1]

[1]Department of Physics & Astronomy, Louisiana State University, Baton Rouge, LA 70803 USA
[2]Departament de Física, EEBE, Campus Diagonal-Besòs and Barcelona Research Center in Multiscale Science and Engineering, Universitat Politècnica de Catalunya, Eduard Maristany, 10-14, 08019 Barcelona, Catalonia SPAIN
[3]Department of Physics, Southern Illinois University, Carbondale, IL 62901 USA

$(MnNiSi)_{1-x}(FeCoGe)_x$ undergoes a magnetostructural phase transition near room temperature that is acutely sensitive to applied hydrostatic pressure, which presents as a marked shift in the martensitic transition temperature (T_M) by about -7.5 K/kbar. The magnetostructural transition can therefore be induced by applied hydrostatic pressure or by magnetic field. The barocaloric and magnetocaloric effects were measured across T_M (for the sample with $x = 0.38$), and the corresponding entropy changes were $+74$ J/kg K ($P = 2.7$ kbar) and -58 J/kg K ($\mu_0 H = 5$ T), respectively. It was observed that the transition entropy change increases with pressure, which results in an enhancement of the barocaloric effect. Our measurements show that the transformed phase fraction associated with magnetostructural transition does not depend on pressure and therefore this enhancement cannot be attributed to a pressure-assisted completion of the phase transformation.

[*]Correspondence to: tapas.sinp@gmail.com

A solid-state caloric effect is defined as a change in entropy or temperature in a material in response to an isothermal or adiabatic variation of an externally applied parameter such as magnetic field, stress, hydrostatic pressure, or electric field. Materials that exhibit solid-state caloric phenomena could promote the development of more environmentally-friendly and efficient alternatives to conventional, vapor-compression-based cooling devices. Significant progress has been made over the past decade in the development of magnetocaloric effects (MCE), and materials that exhibit this property have long been sought for applications in room temperature magnetic cooling [1-5]. However, the less-studied pressure-induced effect, i.e., the barocaloric effect (BCE), has shown promise after recent discoveries of the phenomenon in solid-state materials [6-14]. The BCE is expected to occur in any solid material that undergoes a pressure-induced volume change. In turn, as predicted theoretically, the most likely candidates to show both large BCE and MCE (i.e., multicaloric effects) are materials that undergo a first-order magnetic transition (FOMT) with a simultaneous large change in volume [15]. The combined caloric (multicaloric) effects in a single material may provide a way to improve the effectiveness and efficiency of solid-state cooling. For instance, a pressure-induced shift of a first-order transition may be utilized to overcome the negative consequences of thermal hysteresis [16] and also to modify the operational temperature regimes for cooling [17, 18].

Here we report the observation of a large BCE and MCE at the same FOMT near room temperature in the MnNiSi-based compound, $(MnNiSi)_{1-x}(FeCoGe)_x$ ($x = 0.38$). In recent years, the Mn-based ternary compounds with the formula $MnTX$ (T = Ni, Co and X = Si, Ge) have attracted considerable attention because of their pronounced magnetocaloric properties near room temperature. In these compounds, the effects originate from a magnetostructural transition (MST) with a large volume change of about 3-4% [19-26]. A large volume change is also

responsible for the large MCE in $(MnNiSi)_{1-x}(FeCoGe)_x$ [24]. The large pressure-induced shift of the MST that was observed in our study of the magnetocaloric properties of this compound [24] prompted this current study of its barocaloric properties. In their stoichiometric forms, the materials in this family undergo a second-order magnetic transition with a variety of magnetic structures in the ordered state (depending on composition), such as collinear ferromagnetic (e.g., in MnCoGe and MnNiSi) [27], spiral antiferromagnetic (in MnNiGe) [28], and noncollinear helical antiferromagnetic (in MnCoSi) [29, 30] structures. In the paramagnetic state, all of the compounds undergo a martensitic structural transition from a high-temperature hexagonal Ni_2In-type structure to a low-temperature orthorhombic TiNiSi-type structure accompanied by a positive and large change in volume. In order to obtain large caloric effects, it is crucial that the magnetic and structural transitions be coupled. This can often be accomplished by varying the chemical composition [19], changing the stoichiometry [20, 21], isostructurally substituting [22-24], or by applying pressure [25]. Using these tuning strategies, coupled magnetostructural transitions have been realized in many of these materials near room temperature, along with giant magnetocaloric effects bolstered by a large additional structural contribution to the total isothermal entropy change. Generally, the structural transition responds more quickly to external stimuli than the magnetic transition. Consequently, when magnetocrystalline coupling is present, the magnetostructural transition proceeds at the rate of the purely structural transition. It is important for applications that the MST remains coupled over a wide temperature range that spans room temperature.

Polycrystalline $(MnNiSi)_{1-x}(FeCoGe)_x$ ($x = 0.38$ and 0.39) samples were prepared by melting the constituent elements with purities better than 99.9% in an ultra-high purity argon atmosphere using an RF-furnace. $(MnNiSi)_{1-x}(FeCoGe)_x$ exhibits a drastic structural change as it

goes through a MST, which results in a structural breakdown of the bulk sample into a powder. This powder sample is nothing but the polycrystalline grains of the bulk $(MnNiSi)_{1-x}(FeCoGe)_x$ intermetallic compound as it maintains its physical properties after breakdown. Since the MST is above room temperature (T_M = 338 K at P = 0) for the composition with x = 0.38, the as-cast sample was in powder form. However, the as-cast sample was in bulk form for the composition with x = 0.39 (T_M ~ 300 K) and structural breakdown occurred after thermal cycling (below/above T_M). The as-cast samples were annealed under vacuum for 3 days at 1023 K followed by quenching in cold water. The phase purities of the samples at room temperature were determined using an X-ray diffractometer (XRD) employing Cu K_α radiation. A superconducting quantum interference device magnetometer (SQUID, Quantum Design MPMS) was used to measure the magnetization within the temperature interval of 5-380 K, and in applied magnetic fields up to 5 T. Magnetic measurements under hydrostatic pressure (P) were performed in a commercial BeCu cylindrical pressure cell (Quantum Design). Daphne 7373 oil was used as the pressure transmitting medium. The value of the applied pressure was calibrated by measuring the shift of the superconducting transition temperature of Pb used as a reference manometer (Pb has a critical temperature T_C ~ 7.19 K at ambient pressure) [31]. The isothermal entropy changes (ΔS_{MCE}) due to the magnetocaloric effect were estimated from the isothermal magnetization curves [$M(\mu_0 H)$] using the integrated Maxwell relation, $\Delta S_{MCE} = \int_0^{\mu_0 H} \left(\frac{\partial M}{\partial T}\right)_H \mu_0 dH$. Zero-field heat capacity was measured using a Physical Properties Measurement System (PPMS by Quantum Design) in a temperature range of 2–358 K. Calorimetric measurements with and without the application of hydrostatic pressure were carried out employing a purpose-built calorimeter as described in Ref. [6]. The transition entropy change

(referenced to the low-temperature phase at T_0) was estimated from the calorimetric curves using the relation

$$\Delta S_t(T,P) = S(T,P) - S(T_0,P) = \int_{T_0}^{T} \frac{1}{T} \frac{\dot{Q}(P)}{\dot{T}} \, dT$$

where $\dot{Q}(P)$ and $\dot{T}$ are the heat flux and temperature rate, respectively. Direct measurements of the adiabatic temperature change on the fast release of hydrostatic pressure were performed following the procedure described in Ref. [32]. The adiabatic temperature change during pressurization of the sample was carried out using an another purpose-built set-up. The temperature was measured with a type-J thermocouple that was embedded in a mixture of the powdered sample and a pressure transfer medium (a mixture of methanol and ethanol with a ratio of 4:1). The sample was pressurized to $P > 2$ kbar in about 30 s, and the temperature data were recorded every 0.04 s. The adiabatic temperature change was estimated from the zero-field heat capacity data and the $\Delta S_t(T,P)$ curve following Ref. [7].

(MnNiSi)$_{1-x}$(FeCoGe)$_x$ exhibits a large MCE over a wide temperature range (255 K < T < 338 K) by varying the concentration in a narrow interval (0.38 < x < 0.41), which shifts T_M [24]. In the current study, we selected a composition ($x = 0.38$) with the transition temperature T_M above room temperature ($T_M = 338$ K at $P = 0$), since the MST shifts to lower temperature (i.e., closer to room temperature) with increasing pressure. The temperature dependent magnetization data for 0.1 and 5 T applied magnetic fields, and for different applied hydrostatic pressures (under $\mu_0 H = 0.1$ T), are shown in Fig. 1(a). Calorimetric curves for different hydrostatic pressures are shown in Fig. 1(b). The opposite shifts in the MST with applied pressure (negative shift of T_M) and magnetic field (positive shift of T_M) are associated with the stabilization of the high-temperature, low-volume hexagonal phase with pressure and the low-temperature ferromagnetic orthorhombic phase with magnetic field, respectively. These opposing effects of

5

pressure and magnetic field on the magnetocrystalline coupling are responsible for the inverse BCE (positive isothermal entropy change upon applying/increasing pressure) and conventional MCE (negative isothermal entropy change upon applying/increasing magnetic field), respectively.

The endothermic peaks in the heating cycle of the differential scanning calorimetry data (Fig. 1(b)) are a measure of the latent heat of the transition. The latent heat at ambient pressure, calculated as the area beneath the heating curve, is equal to 21 kJ/kg (152 J/cm^3) and corresponds to a transition entropy change of ΔS_t = 62 J/kg K (452 mJ/cm^3 K). Changes in the pressure dependent transition entropy as a function of temperature were calculated from the calorimetric curves and shown in Fig. 2. Interestingly, the total transition entropy change increases from about 62 ± 2 to 74 ± 4 J/kg K with increasing pressure, i.e., a difference of about 12 J/kg K ≡ 88 mJ/cm^3 K as P goes from 0 to 2.7 kbar. The transition temperature shifts to lower temperature with increasing hydrostatic pressure at a rate of dT_M/dP = −7.5 ± 0.5 K/kbar (see the inset of Fig. 2).

The temperature dependence of the pressure-induced entropy change (ΔS_{BCE}) was calculated from the difference between the transition entropy curves (Fig. 2) at pressures P ($\Delta S_t(T,P)$) and P = 0 ($\Delta S_t(T,0)$). The results shown in Fig. 3(a) indicate a large inverse BCE near room temperature. Notably, ΔS_{BCE} increases with increasing pressure up to the highest applied pressure, and its maximum value is significantly larger than the transition entropy at ambient pressure ($\Delta S_t(T,0)$ = 62 J/kg K). The maximum value of ΔS_{BCE}^{max} at P = 2.7 kbar is 74 ± 4 J/kg K with a reversible change of 57 ± 4 J/kg K calculated as the overlap of the entropy curves on heating and cooling. For devices it is desirable to have the largest possible entropy change in the smallest possible volume and, therefore, it is useful to compare materials based on entropy

6

density [4]. The BCE in terms of entropy density for $(MnNiSi)_{1-x}(FeCoGe)_x$ with $x = 0.38$ (540 ± 4 mJ/cm^3 K for $P = 2.7$ kbar) exceeds values reported for the best performing materials as summarized in Table I. The relative cooling power (RCP = $|\Delta S_{BCE}^{max} \times$(FWHM of $\Delta S_{BCE}(T))|$) is another important parameter used to estimate the applicability of a material for solid-state cooling. Calculated from the $\Delta S_{BCE}(T)$ curves in Fig. 3(a), the RCP is 1500 J/kg (11 J/cm^3) for $P = 2.7$ kbar (see the inset of Fig. 3(a)).

The important feature that renders $(MnNiSi)_{1-x}(FeCoGe)_x$ a multicaloric system is that it also exhibits a large magnetocaloric (magnetic-field-induced) effect at the same transition responsible for the large BCE. The field-induced isothermal entropy change (ΔS_{MCE}) is -58 J/kg K (or -425 mJ/cm^3 K) for a field change of $\mu_0 H = 5$ T (Fig. 3(b)) as calculated from magnetization isotherms using a Maxwell relation. The value of ΔS_{MCE} was also determined using the Clausius-Clapeyron equation following Ref. [34], $[\frac{\Delta S}{\Delta M} = -\frac{\mu_0 dH}{dT} \rightarrow \Delta S \sim -(\Delta M/\Delta T)\mu_0 \Delta H$] resulting in $\Delta S_{MCE} = -57$ J/kg K for $\mu_0 H = 5$ T ($\Delta M = 68$ A m^2/kg and $\Delta T = 6$ K for $\mu_0 H = 5$ T). This value is comparable to or larger than those reported for the best magnetocaloric materials known to date (see Table I).
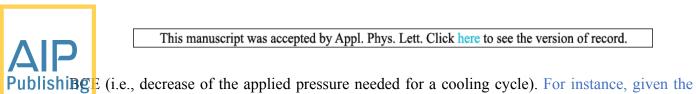
In order to fully characterize the BCE, the adiabatic temperature change must also be known. We have measured the pressure-induced adiabatic temperature change (ΔT_{BCE}) upon compression and decompression, and also estimated it using heat capacity data. An indirect method to estimate ΔT_{BCE} following Ref. [7] is to use zero-field heat capacity data (inset of Fig. 4(a)) and the $\Delta S_t(T,P)$ curve (Fig. 2), giving $|\Delta T|_{BCE} = 16$ K for $P = 2.7$ kbar as shown in Fig. 4(a) (consistent with the 20 K shift of the transition temperature for this applied pressure).

Just as the indirect methods likely overestimate ΔT_{BCE}, direct measurements underestimate it due to non-adiabatic conditions that result in heat flow to and from the

7

surroundings. In our case, direct decompression measurements (see Ref. [32] for details of the experimental system) with P = 2.0 kbar resulted in $\Delta T_{BCE} \sim 3.1$ K (Fig. 4(a)). An experimental set-up was also constructed that measures the direct temperature change on *compression* using large sample masses (> 20 g). Compression-temperature measurements were conducted on a material of slightly different concentration, x = 0.39 rather than 0.38, so that the transition occurred near room temperature (the home-built device could not operate above room temperature). Other than the lower transition temperature ($T_M \sim 300$ K), the material with x = 0.39 behaved nearly identically to that with x = 0.38. The ΔT_{BCE} value on compression for the sample with x = 0.39 was greater than −4.3 K for P = 2.5 kbar at T = 295 K, confirming the negative temperature change on compression due to the inverse BCE. In both cases, compression and decompression, the values of ΔT_{BCE} are comparable to the magnetic-field-induced adiabatic temperature changes reported for giant magnetocaloric materials with $\mu_0 H$ = 2 T (Table I).

Because of the powder form of $(MnNiSi)_{1-x}(FeCoGe)_x$ it is difficult to determine the magnetic-field-induced ΔT_{MCE} accurately by employing direct measurements, or indirectly using field-dependent heat capacity data. In the future, a noncontact method using a pulsed magnetic field could be implemented to determine ΔT_{MCE} as proposed in Ref. [35]. However, the shift in T_M by 6 K for $\mu_0 H$ = 5 T indicates that a $\Delta T_{MCE} \sim 2.4$ K could be expected for $\mu_0 H$ = 2 T. As shown in Fig. 4(b), an increase in the width of the working temperature range, i.e., an effective increase in the cooling efficiency, is possible by applying a magnetic field during depressurization and vice versa. In other words, the range increases if both pressure and magnetic field can be implemented in a cooling cycle, and the temperature changes due to the MCE and BCE may be added [15]. Alternatively, application of a magnetic field during compression will reduce the effective hysteresis [16] and hence enhance the reversibility of the

BCE (i.e., decrease of the applied pressure needed for a cooling cycle). For instance, given the hysteresis of ~15 K, the reversible BCEs will be achieved above $P \sim (15\ K)/(dT_M/dP) \sim 2$ kbar (where $|(dT_M/dP)| = 7.5$ K/kbar) [36]. The application of a 2 T magnetic field together with hydrostatic pressure will effectively decrease the required pressure to observe reversible BCE by about 0.4 kbar by reducing the thermal hysteresis of by ~3 K (highlighted in Fig. 4(b)). This is where multicaloric materials may have a large impact.

In summary, $(MnNiSi)_{1-x}(FeCoGe)_x$ ($x = 0.38$) exhibits both a large BCE and MCE near room temperature that are comparable with or exceed the best multicaloric materials known so far. The combined caloric effects could be employed to optimize the solid-state cooling efficiency desirable for practical applications. Interestingly, the transition entropy change increases with pressure, which is an unusual feature among magnetostructural alloys and compounds that leads to an enhancement of the barocaloric effect above the transition entropy change at normal pressure.

References:

[1] V. K. Pecharsky, and K. A. Gschneidner Jr., Phys. Rev. Lett. **78**, 4494 (1997).

[2] O. Tegus, E. Brück, K. H. J. Buschow, and F. R. de Boer, Nature **415**, 150 (2002).

[3] T. Krenke, E. Duman, M. Acet, E. F. Wassermann, X. Moya, L. Mañosa, and A. Planes, Nat. Mater. **4**, 450 (2005).

[4] K. A. Gschneidner Jr., V. K. Pecharsky, and A. O. Tsokol, Rep. Prog. Phys. **68,** 1479 (2005).

[5] X. Moya, S. Kar-Narayan, and N. D. Mathur, Nat. Mater. **13**, 439 (2014).

[6] L. Mañosa, D. González-Alonso, A. Planes, E. Bonnot, M. Barrio, J.-L. Tamarit, S. Aksoy, and M. Acet, Nat. Mater. **9**, 478 (2010).

[7] D. Matsunami, A. Fujita, K. Takenaka, and M. Kano, Nat. Mater. **14**, 73 (2015).

[8] P. Lloveras, E. Stern-Taulats, M. Barrio, J. L. Tamarit, S. Crossley, W. Li, V. Pomjakushin, A. Planes, L. Mañosa, N. D. Mathur, and X. Moya, Nat. Commun. **6**, 8801 (2015).

[9] S. Crossley, N. D. Mathur, and X. Moya, AIP Advances **5**, 067153 (2015).

[10] R. R. Wu, L. F. Bao, F. X. Hu, H. Wu, Q. Z. Huang, J. Wang, X. L. Dong, G. N. Li, J. R. Sun, F. R. Shen, T. Y. Zhao, X. Q. Zheng, L. C. Wang, Y. Liu, W. L. Zuo, Y. Y. Zhao, M. Zhang, X. C. Wang, C. Q. Jin, G. H. Rao, X. F. Han, and B. G. Shen, Sci. Rep. **5**, 18027 (2015).

[11] E. Stern-Taulats , A. Planes , P. Lloveras , M. Barrio , J. L. Tamarit , S. Pramanick , S. Majumdar , C. Frontera , and L. Mañosa, Phys. Rev. B **89**, 214105 (2014).

[12] E. Stern-Taulats, A. Gràcia-Condal, A. Planes, P. Lloveras, M. Barrio, J. L. Tamarit, S. Pramanick,   S. Majumdar, and L. Mañosa, Appl. Phys. Lett. **107**, 152409 (2015).

[13] J. M. Bermúdez-García, M. Sánchez-Andújar, S. Castro-García, J. López-Beceiro, R. Artiaga, and M. A. Señarís-Rodríguez, Nat. Commun. **8**, 15715 (2017).

[14] L. Mañosa, and A. Planes, Adv. Mater. **29**, 1603607 (2017).

10

[15] N. A. de Oliveira, Appl. Phys. Lett. **90**, 052501 (2007).

[16] J. Liu, T. Gottschall, K. P. Skokov, J. D. Moore, and O. Gutfleisch, Nat. Mater. **11**, 620 (2012).

[17] L. Mañosa, X. Moya, A. Planes, O. Gutfleisch, J. Lyubina, M. Barrio, J.-L. Tamarit, S. Aksoy, T. Krenke, and M. Acet, Appl. Phys. Lett. **92**, 012515 (2008).

[18] Y. Sun, Z. Arnold, J. Kamarad, G. J. Wang, B. G. Shen, and Z. H. Cheng, Appl. Phys. Lett. **89**, 172513 (2006).

[19] E. Liu, W. Wang, L. Feng, W. Zhu, G. Li, J. Chen, H. Zhang, G. Wu, C. Jiang, H. Xu, and F. de Boer, Nat. Commun. **3**, 873 (2012).

[20] Y. Liu, F. R. Shen, M. Zhang, L. F. Bao, R. R. Wu, Y. Y. Zhao, F. X. Hu, J. Wang, W. L. Zuo , J. R. Sun, and B. G. Shen, J. Alloys Compd. 6**49**, 1048 (2015).

[21] E. K. Liu, W. Zhu, L. Feng, J. L. Chen, W. H. Wang, G. H. Wu, H. Y. Liu, F. B. Meng, H. Z. Luo, and Y. X. Li, Europhys. Lett. **91**, 17003 (2010).

[22] C. L. Zhang, D. H.Wang, Z. D. Han, B. Qian, H. F. Shi, C. Zhu, J. Chen, and T. Z. Wang, Appl. Phys. Lett. **103**, 132411 (2013).

[23] T. Samanta, D. L. Lepkowski, A. Us Saleheen, A. Shankar, J. Prestigiacomo, I. Dubenko, A. Quetz, I. W. H. Oswald, G. T. McCandless, J. Y. Chan, P. W. Adams, D. P. Young, N. Ali, and S. Stadler, Phys. Rev. B **91**, 020401(R) (2015).

[24] T. Samanta, D. L. Lepkowski, A. U. Saleheen, A. Shankar, J. Prestigiacomo, I. Dubenko, A. Quetz, I. W. H. Oswald, G. T. McCandless, J. Y. Chan, P. W. Adams, D. P. Young, N. Ali, and S. Stadler, J. Appl. Phys. **117**, 123911 (2015).

[25] S. Anzai, and K. Ozawa, Phys. Rev. B **18**, 2173 (1978).

[26] N. T. Trung, L. Zhang, L. Caron, K. H. J. Buschow, and E. Brück, Appl. Phys. Lett. **96**, 172504 (2010).

[27] A. SzytuŁa, A. T. Pędziwiatr, Z. Tomkowicz, and W. Bażela, J. Magn. Magn. Mater. **25**, 176 (1981).

[28] W. Bażela, A. Szytuła, T. Todorović, Z. Tomkowicz, and A. Zieba, Phys. Status Solidi A **38**, 721 (1976).

[29] S. Nizioł, R. Fruchart, and J. P. Senateur, Phys. Status Solidi A **51**, K23 (1979).

[30] S. Nizioł, R. Zach, J. P. Senateur, and J. Beille, J. Magn. Magn. Mater. **79**, 333 (1989).

[31] A. Eiling, and J. S. Schilling, J. Phys. F **11**, 623 (1981).

[32] S. Yüce , M. Barrio , B. Emre , E. Stern-Taulats , A. Planes , J. L. Tamarit , Y. Mudryk , K. A. Gschneidner , V. K. Pecharsky , and L. Mañosa, Appl. Phys. Lett. **101**, 071906 (2012).

[33] L. Mañosa , D. González-Alonso , A. Planes , M. Barrio , J. L. Tamarit , I. S. Titov , M. Acet , A. Bhattacharyya , and S. Majumdar, Nat. Commun. **2**, 595 (2011).

[34] R. Kainuma, Y. Imano, W. Ito, Y. Sutou, H. Morito, S. Okamoto, O. Kitakami, K. Oikawa, A. Fujita, T. Kanomata, and K. Ishida, Nature **439**, 957 (2006).

[35] R. Z. Levitin, V. V. Snegirev, A. V. Kopylov, A. S. Lagutin, and A. Gerber, J. Magn. Magn. Mater. **170**, 223 (1997).

[36] B. Emre, S. Yüce, E. Stern-Taulats, A. Planes, S. Fabbrici, F. Albertini, and L. Mañosa, J. Appl. Phys. **113**, 213905 (2013).
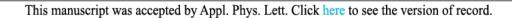
Figure Captions:

Fig. 1(a) Temperature dependence of the magnetization (M) with $\mu_0 H = 0.1$ T for different applied hydrostatic pressures (P) and at ambient pressure for (MnNiSi)$_{1-x}$(FeCoGe)$_x$ ($x = 0.38$) (left axis). $M(T)$ for 5 T applied magnetic field (Red line and symbols) is referred to the right axis. The dotted arrows indicate the shifts of the transition with pressure and magnetic field. (b) Calorimetric heat flow curves (dq/dT) for selected values of hydrostatic pressure.

Fig. 2 Pressure dependent transition entropy as a function of temperature. Entropy change (ΔS_t) relative to the low-temperature phase for selected applied hydrostatic pressures (P). From left to right, the curves correspond to 2.7, 2.4, 2.1, 1.9, 1.6, 1.2, 1.1, 0.8, 0.5, and 0 kbar. The error bars are shown for the maximum pressure (± 4 J/kg K) and for normal pressure (± 2 J/kg K). The error bars for the remaining curves are the same as for that at the highest pressure. The inset shows the temperature shifts in the peaks of the calorimetric curves as a function of applied pressure.

Fig. 3 Entropy changes associated with (a) barocaloric and (b) magnetocaloric effects with the application of pressures up to 2.7 kbar and magnetic fields up to 5 T, respectively. The error bar for the maximum BCE (± 4 J/kg K) is shown and is valid for any pressure. The inset of (a) shows the relative cooling power (RCP = $|\Delta S_{\text{BCE}}^{max} \times$(FWHM of $\Delta S_{\text{BCE}}(T))|$) as a function of pressure. The error in the RCP is ± 4 J/kg for the maximum pressure and is valid for any pressure. No error bars are shown as they are smaller than the symbol size.

Fig. 4(a) The adiabatic temperature change upon depressurization from 2 kbar to atmosphere (right axis), and the same estimated from zero-field heat capacity data (left axis). The heat capacity as a function of temperature is shown in the inset. (b) The pressure-induced entropy change for $P = 2.7$ kbar and the magnetic-field-induced change for $\mu_0 H = 2$ T plotted to illustrate

the potential extension of the width of the entropy versus temperature curve that might be

realized by a cooling cycle that employs both hydrostatic pressure and magnetic field.

TABLE I. Materials exhibiting giant multicaloric effects at first-order phase transitions including $(MnNiSi)_{1-x}(FeCoGe)_x$ with $x = 0.38$ (present work). Isothermal entropy change $|\Delta S|$, adiabatic temperature change $|\Delta T|$, and relative cooling power RCP, due to changes of hydrostatic pressure P (barocaloric, BCE) and magnetic field $\mu_0 H$ (magnetocaloric, MCE). Entries inside curly brackets {…} were derived from direct measurements. *Data acquired from hydrostatic decompression measurements. †Data acquired from hydrostatic compression measurement using a slightly different concentration $x = 0.39$. #Data derived from direct measurement by pressurizing the sample using a hydraulic press. Entries inside round brackets (…) denote parameters derived from $-c\Delta T \approx T\Delta S$ using zero-field heat capacity data. Entries in italic font signify data derived from quasi-direct measurements. No data was available for the dashed entries. The mass density is ρ.

Materials	T	$|\Delta S|_{BCE}$	$|\Delta T|_{BCE}$	RCP	P	$|\Delta S|_{MCE}$	$|\Delta T|_{MCE}$	RCP	$\mu_0 H$	ρ	References
	K	mJ/cm³ K	K	J/cm³	kbar	mJ/cm³ K	K	J/cm³	T	g/cm³	
$Ni_{49.26}Mn_{36.08}In_{14.66}$	293	200	(4.5)	1	2.6	82	(1.3)	0.3	0.94	8.2	[6]
$Gd_5Si_2Ge_2$	270	82.5	{1.1}*	1	2.9*	120	(7)	0.96	2	7.5	[1, 32]
$LaFe_{11.33}Co_{0.47}Si_{1.2}$	237	63.5	{2.2}*	1.3	2.0*	76	{0.9}	0.33	5 1	7.3	[33]
$Fe_{49}Rh_{51}$	308	123.5	(8.1)	1	1.1	120	(6)	2.5	2	9.8	[11, 12]
$MnCoGe_{0.99}In_{0.01}$	308	413	(18.5) {9.4}#	9.5	3.0 3.0#	95	(2.8)	0.63	2	7.95	[10, 20]
Mn_3GaN	285	170	(4.8)	1.5	1.39	–	–	–	–	7.6	[7]
$(NH_4)_2SO_4$	219	106	(8)	0.5	1.0	–	–	–	–	1.8	[8]
$(MnNiSi)_{0.62}(FeCoGe)_{0.38}$	338	538	{3.1}* {4.3}† (16)	11	2.0* 2.5† 2.7	152	(2.4)	0.9	2	7.3	Present work